AGU ADVANCING EARTH AND SPACE SCIENCES

JGR Atmospheres

RESEARCH ARTICLE
10.1029/2024JD041296

Evolution of the Climate Forcing During the Two Years After the Hunga Tonga-Hunga Ha'apai Eruption

M. R. Schoeberl[1], Y. Wang[1], G. Taha[2], D. J. Zawada[3], R. Ueyama[4], and A. Dessler[5]

[1]Science and Technology Corporation, Columbia, MD, USA, [2]Morgan State University, Baltimore, MD, USA, [3]Institute of Space and Atmospheric Studies, University of Saskatchewan, Saskatoon, SK, Canada, [4]NASA Ames Research Center, Moffett Field, CA, USA, [5]Texas A&M University, College Station, TX, USA

Key Points:

- The 15 Jan. 2022, Hunga eruption increased aerosols and H_2O in the southern hemisphere stratosphere and then dispersed throughout 2022/3
- Stratospheric water vapor, ozone, temperature, and aerosol optical depth contribute to the change in downward radiative fluxes
- Hunga produced a global decrease in radiative of less than ~0.25 W/m^2 over the 2 yrs period

Correspondence to:
M. R. Schoeberl,
mark.schoeberl@mac.com

Citation:
Schoeberl, M. R., Wang, Y., Taha, G., Zawada, D. J., Ueyama, R., & Dessler, A. (2024). Evolution of the climate forcing during the two years after the Hunga Tonga-Hunga Ha'apai eruption. *Journal of Geophysical Research: Atmospheres*, *129*, e2024JD041296. https://doi.org/10.1029/2024JD041296

Received 3 APR 2024
Accepted 10 JUL 2024

Author Contributions:
Conceptualization: M. R. Schoeberl, G. Taha
Data curation: M. R. Schoeberl, D. J. Zawada
Formal analysis: M. R. Schoeberl, Y. Wang
Funding acquisition: M. R. Schoeberl, R. Ueyama, A. Dessler
Investigation: M. R. Schoeberl, G. Taha
Methodology: M. R. Schoeberl, G. Taha, A. Dessler
Project administration: M. R. Schoeberl, R. Ueyama
Software: M. R. Schoeberl, Y. Wang
Validation: M. R. Schoeberl, Y. Wang
Writing – original draft: M. R. Schoeberl
Writing – review & editing: M. R. Schoeberl, Y. Wang, G. Taha, D. J. Zawada, R. Ueyama, A. Dessler

Abstract We calculate the climate forcing for the 2 ys after the 15 January 2022, Hunga Tonga-Hunga Ha'apai (Hunga) eruption. We use satellite observations of stratospheric aerosols, trace gases and temperatures to compute the tropopause radiative flux changes relative to climatology. Overall, the net downward radiative flux decreased compared to climatology. The Hunga stratospheric water vapor anomaly initially increases the downward infrared radiative flux, but this forcing diminishes as the anomaly disperses. The Hunga aerosols cause a solar flux reduction that dominates the net flux change over most of the 2 yrs period. Hunga induced temperature changes produce a decrease in downward long-wave flux. Hunga induced ozone reduction increases the short-wave downward flux creating small sub-tropical increase in total flux from mid-2022 to 2023. By the end of 2023, most of the Hunga induced radiative forcing changes have disappeared. There is some disagreement in the satellite measured stratospheric aerosol optical depth (SAOD) observations which we view as a measure of the uncertainty; however, the SAOD uncertainty does not alter our conclusion that, overall, aerosols dominate the radiative flux changes.

Plain Language Summary The Hunga Tonga-Hunga Ha'apai (Hunga) submarine volcanic eruption on 15 January 2022, produced aerosol and water vapor plumes in the stratosphere. These plumes have persisted mostly in the Southern Hemisphere throughout 2022 and into 2023. Enhanced tropospheric warming due to the added stratospheric water vapor is offset by the larger stratospheric aerosol attenuation of solar radiation. Hunga induced circulation changes that reduce stratospheric ozone and lower temperatures also play a role in the net forcing. The change in the radiative flux would result in a very slight 2022/3 cooling in Southern Hemisphere. The Hunga climate forcing has decreased to near zero by the end of 2023.

1. Introduction

The eruption of the Hunga Tonga-Hunga Ha'apai (Hunga) (20.54°S, 175.38°W) submarine volcano on 15 Jan. 2022, sent material to the mesosphere (Carr et al., 2022; Proud et al., 2022). Microwave Limb Sounder (MLS) measurements (Millán et al., 2022; Millán et al., 2024 hereafter M22, M24; Santee et al., 2023) and balloon sondes measurements (Vomel et al., 2022) showed that a significant amount of water vapor was injected by the eruption into the tropical Southern Hemisphere (SH) mid-stratosphere. The MLS measured Hunga water injection was estimated to be 146 Tg or ~10% of the total stratospheric water vapor (M22). The water vapor anomaly has persisted throughout 2,022 and 2,023 (M24). The presence of water vapor led to a tropical stratospheric cooling of ~4 K in March and April (Schoeberl et al., 2022, hereafter S22) due to the increased outgoing IR radiation. This cooling produces a secondary circulation (Coy et al., 2022) that decreased extra-tropical temperatures and ozone (Wang et al., 2023) in mid 2,022.

Hunga also injected at least 0.5 Tg of SO_2 into the stratosphere (Carn et al., 2022) although this amount may have been as much as 1.5 Tg (Sellitto et al., 2024). SO_2 oxidation forms a sulfate aerosol layer that was detected by the Ozone Mapping and Profile Suite limb profiler (OMPS) (Taha et al., 2022) shortly after the eruption. Volcanically generated increases in stratospheric aerosols cause a reduction in solar radiative forcing and, if large enough, can produce an observable decrease in tropospheric temperatures (Aubry et al., 2021; Crutzen, 2006; Fujiwara et al., 2020; Hansen et al., 2002; Robock, 2000; Santer et al., 2001; Stenchikov, 2016). Volcanic aerosols can persist in the stratosphere for years and even self-loft through solar heating when the aerosols are mixed with ash (Khaykin et al., 2022).

Changes in stratospheric water vapor can also cause changes in climate forcing (Forster & Shine, 1999). Solomon et al. (2010) showed that the lower tropical stratospheric decrease of ∼0.4 ppmv H_2O between 2,000 and ∼2,005 would reduce tropospheric forcing by ∼0.098 W/m^2 or about ∼0.245 W/m^2/ppmv. The water vapor radiative forcing results from changes in the thermal IR emission and solar flux absorption. The radiative forcing due to solar flux absorption is generally smaller than that due to thermal emission. Extending the Solomon et al. (2010) study, Dessler et al. (2013) calculated a water vapor climate feedback parameter of 0.27 W/m^2/ppmv. Banerjee et al. (2019) analyzing CMIP5 models computed the stratospheric water vapor component of the climate feedback parameter to be 0.14 W/m^2/K for 4xCO_2. Li and Newman (2020) using the Goddard Earth Observing System Chemistry-Climate model computed a similar 4xCO_2 stratospheric water vapor feedback value of 0.11 W/m^2/K.

Given the sensitivity of the climate to stratospheric water vapor, it is logical to assume that Hunga's water vapor injection might have a significant climate impact. Jenkins et al. (2023) used a parameterized climate-response model to investigate the climate impact of the Hunga water vapor plume. They neglected the impact of aerosols and only considered the radiative forcing due to the water vapor injection and computed a 0.12 W/m^2 increase in tropospheric radiative forcing. However, Sellitto et al. (2022) and Zhu et al. (2022) roughly estimated that the aerosol plume would produce a peak February solar forcing reduction of ∼1.7 and 2.1 W/m^2, exceeding the estimated forcing increase due to H_2O. Schoeberl, Wang, Ueyama, Dessler, et al., 2023 hereafter S23b) provided a more accurate estimate of the aerosol and water vapor forcing confirming that the aerosol forcing overwhelms the water vapor flux increase during the first year following the eruption.

In this study we extend the S23b computation of the radiative forcing into the second year following the Hunga eruption. Our basic approach is the same as S23b, but in addition we break out the various radiative forcing components in more detail. As before we use the OMPS measurements of stratospheric aerosol extinction (Taha et al., 2022) to compute the stratospheric aerosol optical depth (SAOD), but we also compare NASA OMPS SAOD to the Stratospheric Aerosol and Gas Experiment III international space station (SAGE III/ISS) measurements of SAOD, and OMPS data processed using U. of Saskatchewan (USask) algorithm. The USask OMPS data are processed using a tomographic retrieval scheme (Bourassa et al., 2023) that is different from the NASA algorithm. The tomographic retrieval has the advantage of correcting OMPS measurements for distortion around the edges of aerosol and cloud anomalies (see Gorkavyi et al., 2021). The USask retrieval also makes different assumptions about the aerosol size distribution. We refer to these data as USask OMPS.

To estimate the trace gas radiative forcing we use the AER rapid radiative transfer model (RRTM, Mlawer et al., 1997) to compute the changes in shortwave and longwave fluxes at the tropopause. We include solar zenith angle variations in computation of the shortwave fluxes. Our approach is to use the prior 10 yrs climatology (2012–2021) of MLS trace gases and temperatures, compute the radiative forcing, and then swap in the changes observed by MLS in the 2022–2023 period to compute the relative change in radiative forcing. This allows us to quantify the relative importance of various processes contributing to the overall radiative impact relative to the 10 yrs climatology. In general, longwave IR radiation from the mid-stratosphere will be absorbed in the cold upper troposphere whereas shortwave radiation will penetrate to the surface, which means that the tropospheric climate response to the longwave and shortwave radiative forcing changes will be different. That said, the tropospheric climatic response to these flux changes is beyond the scope of this study. Our goal is to determine the net flux changes at the tropopause as the Hunga plume evolves.

2. Observational Data Sets

We use Microwave Limb Sounder (MLS) V5 for temperature and trace gas observations. The data quality for the Hunga anomaly is detailed in M22, and MLS data is described in Livesey et al. (2021). Other trace gases changes are described in Santee et al. (2023). We restrict our constituent analysis to below 35 km well above the maximum Hunga water vapor anomaly (∼25 km). The climate forcing due water vapor emissions above 30 km is negligible (Solomon et al., 2010). The MLS daily data sets are averaged onto a 5° × 10° latitude-longitude grid. The trace gas and temperature climatologies are constructed from 10 years of data (2012–2021).

We use NASA OMPS level-2 V2.1 aerosol extinction data (Taha et al., 2021) which provides aerosol retrievals up to 40 km. Although the extinction measurements by OMPS V2.1 are generally consistent with those made by SAGE III/ISS (Taha et al., 2021), as shown in Gorkavyi et al. (2021), the NASA OMPS algorithm may overestimate the aerosol extinction at the edges and below eruption clouds because of the limb viewing geometry. Bourassa et al. (2023) developed a tomographic retrieval scheme that corrects for the OMPS viewing geometry problems, and the USask OMPS retrieved Hunga extinction levels are roughly a factor of two smaller than NASA OMPS for the first 4 months after the eruption. As Bourassa et al. (2023) noted, the aerosol distribution becomes more zonal after the first 4 months, and the difference between the two extinction estimates becomes smaller.

For both NASA OMPS and USask OMPS, we integrate the 745 nm extinction from 1 km above the tropopause to 35 km to obtain SAOD. We use extinction measurements at 745 nm since this wavelength has good sensitivity to small particles and is less contaminated by Rayleigh scattering than shorter wavelengths (Taha et al., 2021). The tropopause information comes from the Modern-Era Retrospective analysis for Research and Applications, Version 2 (MERRA2, see Gelaro et al., 2017). We start the integration above the tropopause to eliminate the contamination by thin clouds near the tropopause. The zonal mean tropopause is located ~16.5 km between ±20° and is ~8–10 km poleward of that region. Daily aerosol extinction data are interpolated onto a 2° latitude zonal mean daily grid; we use a 10 days box-car smoother to reduce measurement variability.

We use the S23b algorithm to convert SAOD to solar flux reduction; the algorithm uses the 550 nm SAOD. To convert the SAOD at the 745 nm wavelength to 550 nm we use the Ångström exponent from SAGE III/ISS (Cisewski et al., 2014) calculated using extinction coefficients at 550 and 756 nm. We use the SAGE Ångström exponent instead of one derived from OMPS, because the OMPS Ångström exponent appears inconsistent with the SAGE Ångström exponent likely due to limitation of the shorter wavelength retrievals in the lower altitude SH, and, to some extent, the algorithm's particle size assumptions.

3. Analysis of Hunga Climate Impact

3.1. Changes in Constituent Distributions and Temperatures Following Hunga Eruption

To interpret the changes in downward radiative fluxes, we need to assess how the constituent distribution and temperatures change following the eruption relative to climatology. Some of these changes are part of year-to-year variability in the stratosphere (e.g., the quasi-biennial oscillation, QBO), whereas others are induced by the Hunga water vapor and aerosol anomalies. Figure 1 shows the equatorial cross-sectional time series of aerosols, water vapor, ozone, and temperature. Overlaid on each figure is the equatorial zero wind line, showing the descent of the westerly phase of the QBO starting in April 2022, and the easterly phase starting in April 2023.

Figure 1a shows that aerosols enter the tropical region shortly after the Hunga eruption on 15 Jan. 2022. The aerosol concentration gradient follows the zero-wind line downward as the meridional circulation associated with the QBO pushes aerosols southward (Schoeberl, Wang, Ueyama, Taha, & Yu, 2023). In contrast, Figure 1b shows that the water vapor anomaly moves steadily upward as part of the Brewer-Dobson (BD) circulation. The usual tape-recorder signal is also evident in the figure with ascending smaller water vapor anomalies in August 2022 and August 2023.

Associated with the QBO westerly descent Figure 1c shows an ozone increase moving with the zero-wind line. This ozone increase is also associated with the QBO secondary circulation (Plumb & Bell, 1982) which advects higher concentration of ozone downward and creates a warm temperature anomaly seen in Figure 1d. The reverse occurs for the descending QBO easterly phase in 2023.

Figure 2 shows the cross-sectional time series as in Figure 1 but at 40°S. Aerosols and water vapor arrive at this latitude mostly after May 2022. This latitude is too far south to be influenced by the QBO's secondary circulation. However, the water vapor anomaly is strongly correlated with a decrease in ozone and temperature starting in May 2022 and ending in December 2022. Wang et al. (2023) shows that this anomaly is the result of a weakening of the descending branch of the BD circulation due to in situ radiative cooling associated with Hunga water vapor. The descending branch transports ozone from higher altitudes into the middle stratosphere and adiabatically warms the region. As the BD circulation weakens, both an ozone and temperature anomaly form. Later, as the water vapor anomaly disperses, and as the summer SH BD circulation anomaly weakens then fades.

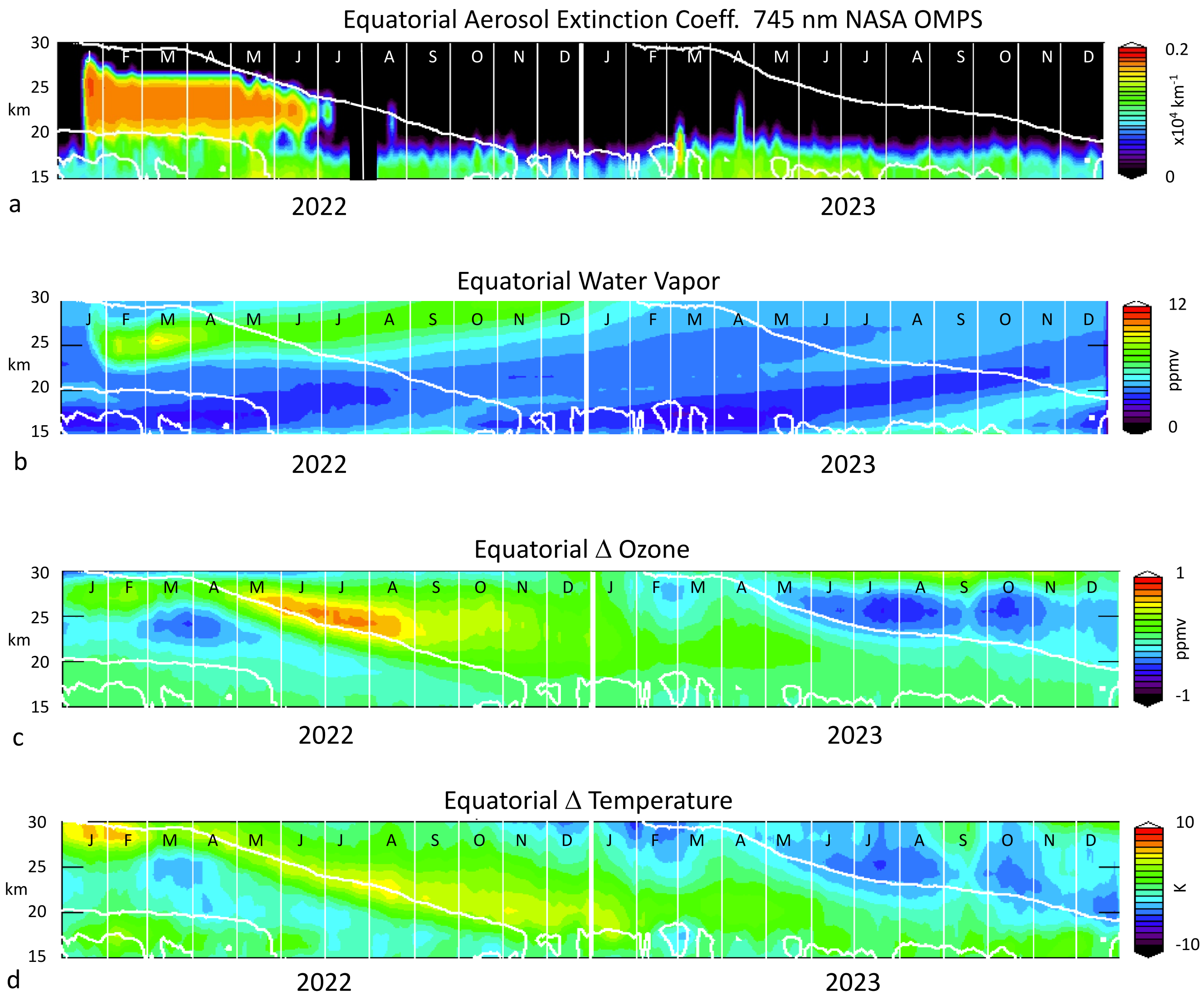

Figure 1. Equatorial cross section of aerosols and trace gases. Part a 745 nm extinction coefficient (km^{-1}) ±1° of the equator. Part b, water vapor, Part c Δ ozone (difference from 10 yrs climatology). Part d, Δ temperature all ±2.5° of the equator. Month letters starting 2,022 are shown in the figure. Months are show as first letters and monthly regions are divided by white lines. The thick white line is the equatorial zero wind line from MERRA2 assimilation. Color bars indicate the scale.

Figure 3 shows OMPS 745 nm aerosol extinction coefficient at 20 km, as well as water vapor at 25 km along with changes in ozone and temperature relative to the 10 yrs MLS climatology at 25 km. This figure provides a third perspective on constituent changes. The aerosol and water vapor anomalies stay isolated in the SH except for some initial transport into the Northern Hemisphere (NH) shortly after the eruption (Schoeberl, Wang, Ueyama, Taha, & Yu, 2023 hereafter S23a). The tropical temperature decrease in Feb.-April 2022 is due to radiative cooling by water vapor (S22). The changes in ozone at the equator—the increase in May-September 2022 and decrease in the same months in 2023 are associated with the QBO circulation moving downward through this altitude region (Figure 1).

In the SH extra-tropics, the March 2022 temperature (Figure 3c) decrease is due to water vapor cooling (S22), but the later temperature and ozone decrease further south is the result of the weakening BD circulation mentioned above (Wang et al., 2023). As indicated above, under normal conditions, the BD circulation adiabatically heats the extra-tropics and advects ozone into the lower stratosphere. The weaker BD circulation thus causes a temperature and ozone decrease.

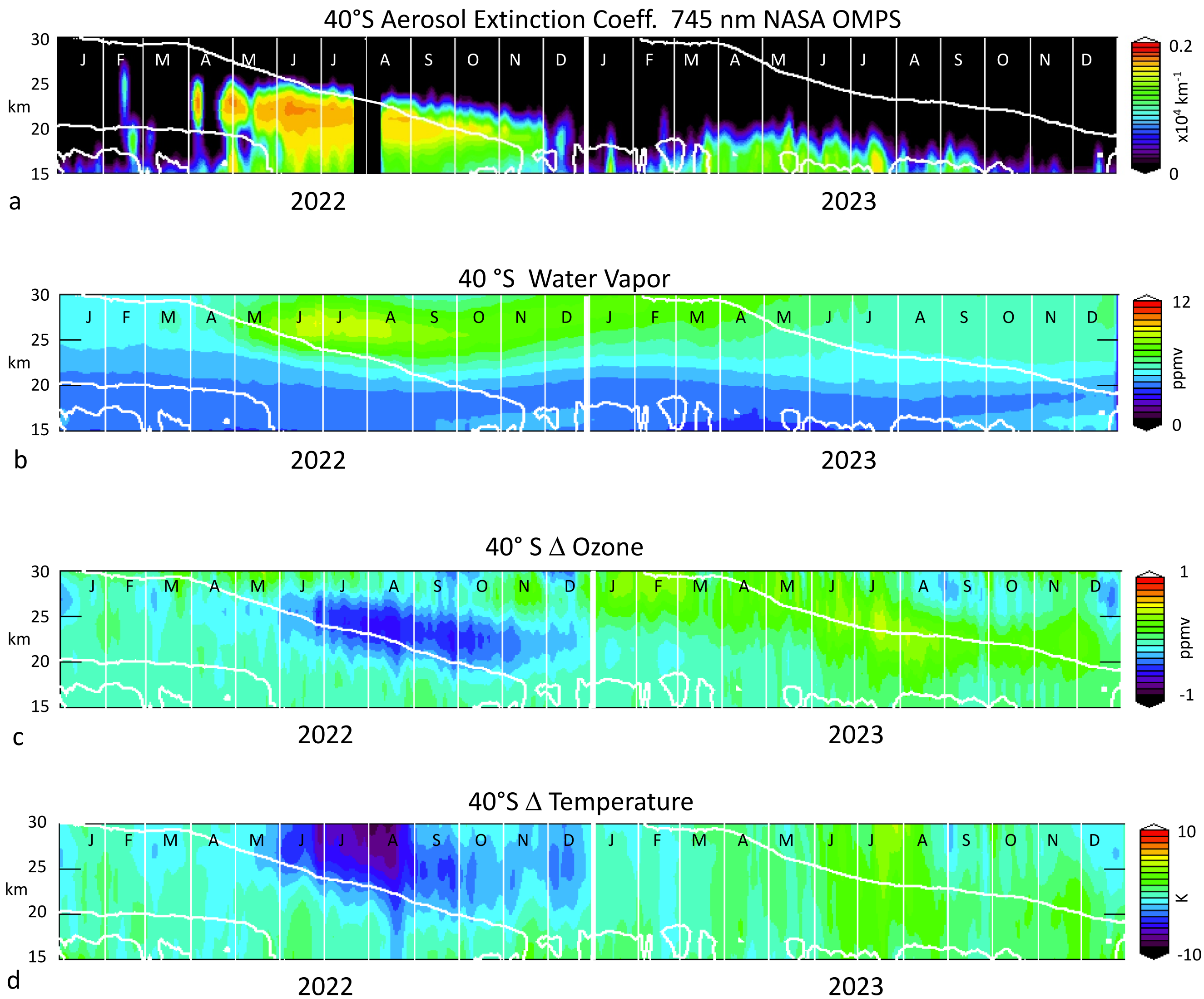

Figure 2. Same as Figure 1 at 40° s.

3.2. Aerosol Direct Forcing

3.2.1. Aerosol Measurements

The S23b parameterization scheme described in Section 2 is used to compute the aerosol direct solar forcing. Solar zenith angle variations are included in the computation. This scheme, as do the schemes shown in Table 1, uses the SAOD at 550 nm derived from extinction measurements at 745 nm and converted to 550 nm using the SAGE Ångström exponent. Figure 4 shows time series of the NASA OMPS 745 nm SAOD (4a), the USask 745 nm SAOD (4b), and SAGE III/ISS 756 nm SAOD (4c). The SAGE measurements are interpolated to the OMPS regular grid, but we show the SAGE measurement points to indicate where the interpolation is filling in missing data. Figure 4d compares the OMPS SAOD measurements converted to 550 nm at 20°S and the SAGE 550 nm SAOD measurements interpolated to the OMPS grid.

Figure 4 shows the range of SAOD values with USask nearly a factor of two smaller than NASA OMPS after the eruption. The main difference between the two OMPS SAOD retrievals is that USask corrects for the effects of inhomogeneity along the line of sight (Bourassa et al., 2023), although differences can also be caused by the difference between size distribution assumptions built into the two algorithms. However, from the SAGE measurements, it is apparent that USask is low biased while the NASA is high biased. Figure 4d shows that after

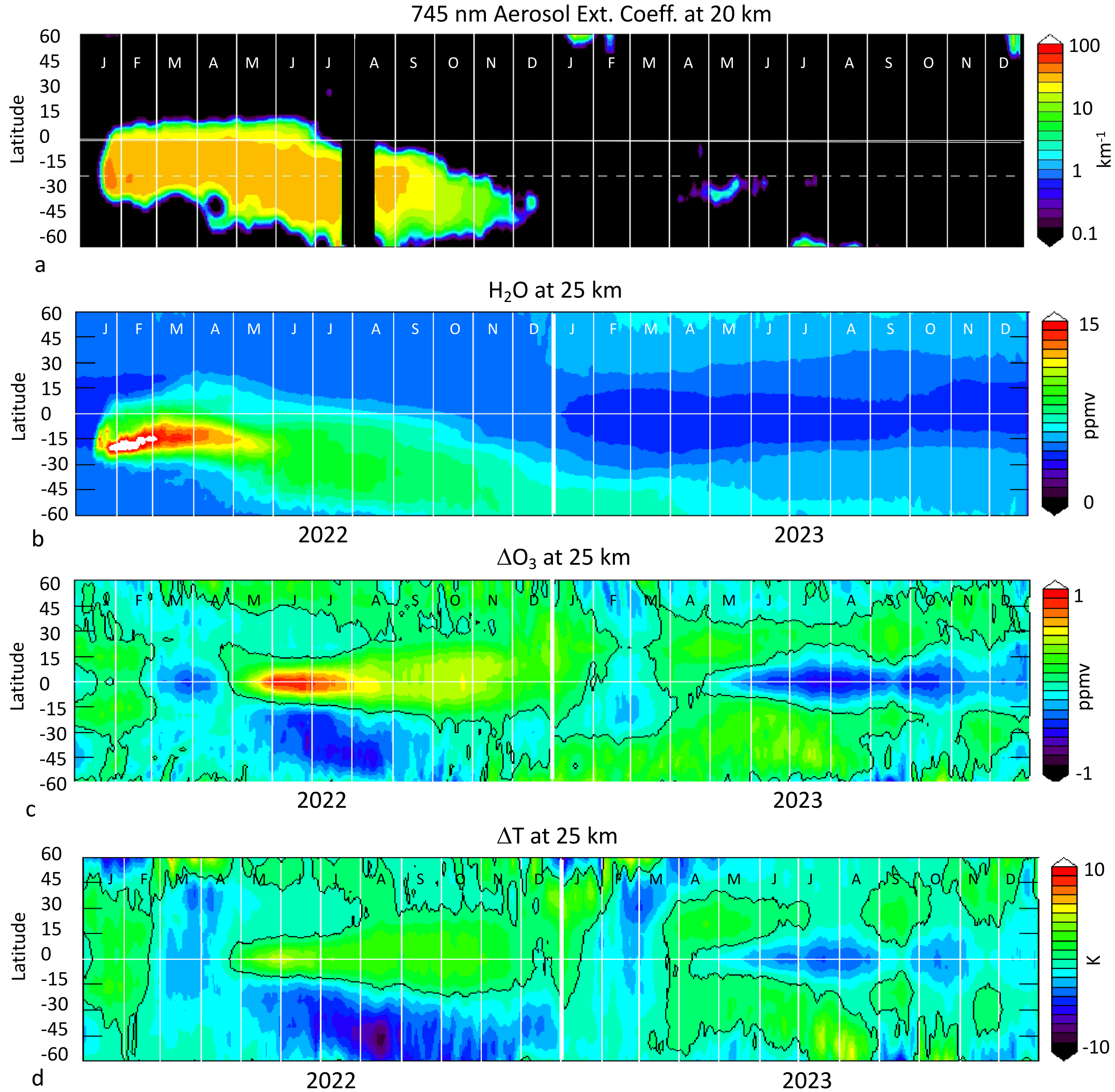

Figure 3. Constituent zonal mean fields. Part a, aerosol extinction coefficient at 20 km from NASA OMPS-LP. Parts b-d MLS at 25 km. Part b, water vapor, Part c Δ ozone, Part c Δ temperature. Thin white horizontal line indicates the equator. Thick black line contour is zero in parts d and (d).

August 2022, NASA OMPS comes into agreement with SAGE and all three SAOD estimates converge in mid-2023 (The slower rise in SAGE SAOD after the eruption is due to the SAGE measurement pattern which missed the initial eruption latitude.) We view the differing SAOD estimates as a measure of the uncertainty. In our forcing estimates below, we will show results with both NASA OMPS SAOD and USask SAOD—which tend to bracket the SAGE estimates.

The evolution of the SAOD (Figure 4) reflects the evolution of the aerosol distribution shown in Figure 3a (also Taha et al., 2022). NASA and USask SAOD distributions both show an initial high value between 30°S and the equator until May-June when the SAOD shifts south. This shift is also apparent in the aerosol distribution at 20 km (Figure 3a). The southward shift is due to increased seasonal eddy transport.

Table 1
Parameterization for SAOD Solar Forcing

Reference	R
Hansen et al. (2002)	21
Yu and Huang (2023)	29.5—Clear 15.7—All sky
Yu et al. (2023)	23
S23b linear-log fit	19.5 SAOD <0.015
	5.58 + 1.26 $\log_e$ (SAOD) SAOD >0.015

An anomaly in the USask SAOD during May/June/July 2022 from 45°S to 60°S is not seen NASA SAOD and is possibly a retrieval artifact. In April-July 2023, NASA OMPS shows a new enhancement in SAOD south of 30° S. This enhancement is much less evident in the USask product. The source of the enhancement is unknown but may be a movement of Hunga polar aerosols back toward mid-latitudes with the formation of the Antarctic polar vortex. No SH volcanic eruptions occurred during this period. Finally, we note that by the end of 2,023 the SAOD anomalies have largely disappeared.

3.2.2. Direct Forcing Parameterization

A variety of parameterizations have been used to convert global averaged SAOD into global average solar direct forcing change (ΔA) as shown in Table 1. These parameterizations take the form ΔA = -R SAOD (550 nm).

The linear parameterizations tend to underestimate the forcing of mid-sized eruptions (e.g., El Chichón, SAOD of ∼0.05) and overestimate very large eruptions (e.g., Pinatubo, SAOD of 0.2, Pitari et al., 2006). The Yu and Huang (2023) parameterization was developed from MERRA2 tropospheric AOD estimates during a non-volcanic period. In their nomenclature, 'Clear' assumes no cloud reflectivity whereas 'All sky' includes climatological cloud distributions. Most estimates of direct solar forcing changes do not include cloud effects because the solar flux impact of clouds is considered a separate uncertainty (Hansen et al., 2002). In this study, we will use the Yu and Huang (2023) algorithm to estimate the impact of clouds on the Hunga direct forcing as was done in S23b. Note that the All sky climatology and does not change with season nor solar zenith angle, and is used only to provide a simplified estimate of how clouds might affect our results. Aerosols and trace gases shortwave forcing includes solar zenith angle changes.

Figure 5 shows the estimated reduction in solar forcing using NASA OMPS and USask OMPS. The southward movement of the aerosol distribution in May 2022 is reflected in the forcing shift. We also see a slight increase in forcing due to the April-July 2023 SAOD enhancement.

3.3. Flux Changes Due To Trace Gases and Temperatures

In S23b we only considered the water vapor shortwave and longwave IR downward flux changes at the tropopause relative to a 5 yrs MLS water vapor climatology. Here we include the changes due to temperature, ozone, and water vapor relative to a 10 yrs MLS climatology. Our approach is to take the 10 yrs climatology of temperature and trace gases, then insert one of the 2,022/3 anomalies fields and compare the changes in tropopause downward fluxes to the climatology. For example, we insert the observed 2,022/3 water vapor anomaly into the climatology and compare the altered downward fluxes to the downward flux climatology. This works well for isolating the effects of the Hunga water vapor since seasonal variations in stratospheric water vapor is normally ∼10% and Hunga anomalies were up to five times larger than the climatology. For ozone and temperature this approach is more problematic since natural changes that may be unrelated to Hunga certainly occur (e.g., the tropical QBO and extra-tropical stratospheric warmings, Veenus et al., 2023; Tao et al., 2015).

3.3.1. Water Vapor

The Hunga stratospheric water vapor anomaly will increase the tropopause downward long-wave IR flux and reduce the short-wave flux (Solomon et al., 2010). Figure 3a shows the zonal mean water vapor anomaly at 25 km, and Figure 6 shows the corresponding changes in downward flux at the tropopause. The longwave increase is shown in Figure 6a and the shortwave decrease is shown in Figure 6b. After an initial strong LW and SW forcing changes, the impact decreases. The total global Hunga stratospheric water vapor enhancement has remained relatively constant through 2,022/3. But, by the end of 2,023 much of the plume has spread globally and most of the plume is well above 35 km (M24). The spread of the plume reduces the water vapor concentration and this explains the decrease in radiative impact.

The decrease in H_2O shortwave flux is much smaller than the increase in longwave flux. Reduces the direct solar forcing. Figure 6b shows that the H_2O increased long wave flux is on the order of ∼0.6 W/m^2 which is smaller than the aerosol reduction of direct solar forcing (Figure 5).

10.1029/2024JD041296

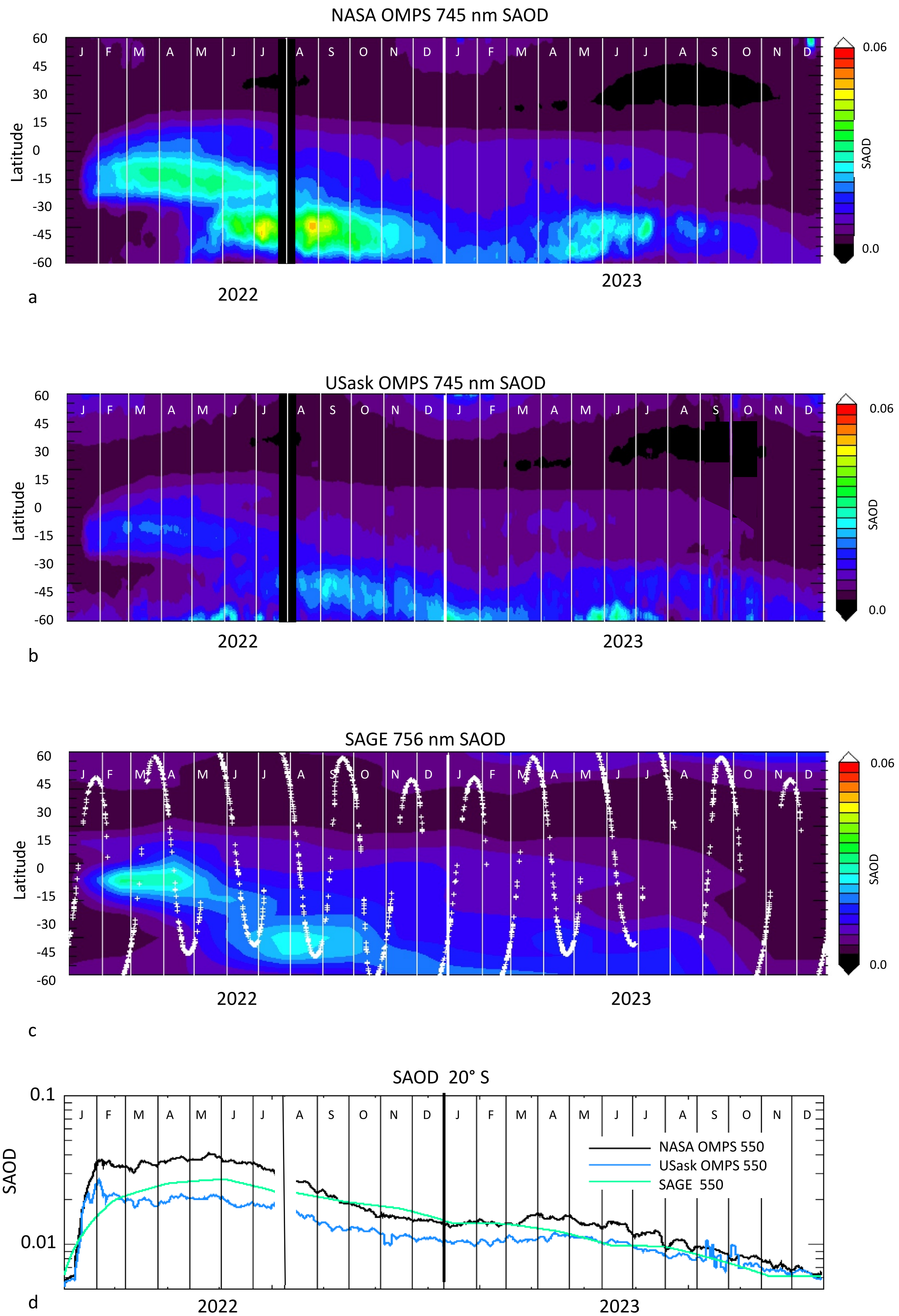

Figure 4. Zonal mean SAOD time series. Part a, NASA OMPS, Part b, USask OMPS, both at 745 nm. Part c, SAGE III/ISS SAOD at 756 nm interpolated onto the OMPS grid. Part d shows the 20°S SAOD converted to 550 nm using the SAGE Ångström exponent from Parts a, b, and (c).

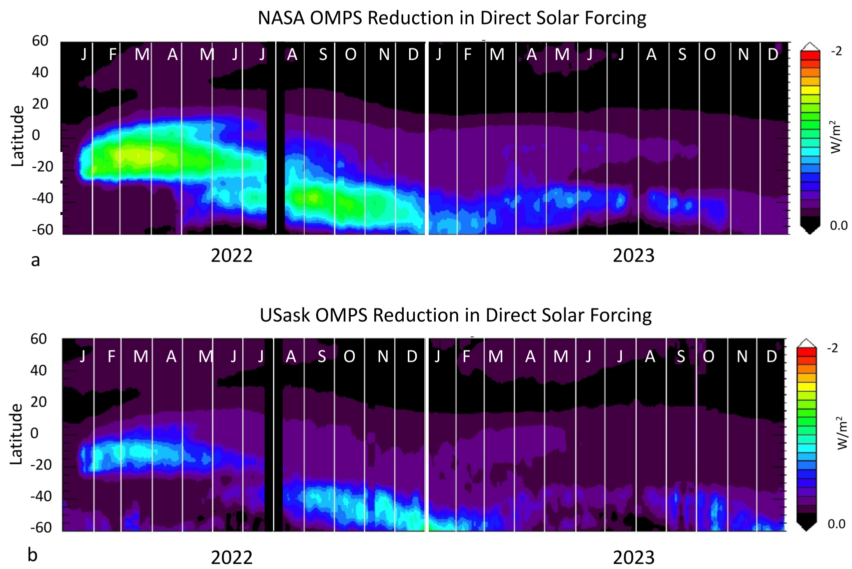

Figure 5. Part a, direct forcing from NASA OMPS SAOD. Part b, direct forcing using USask SAOD.

3.3.2. Ozone

Figure 3b shows the changes in ozone concentration at 25 km between 2022/3 and the climatology. Figure 7 shows the differences in the downward flux. The differences in stratospheric ozone are mostly determined by changes in the transport circulation (Santee et al., 2023; Wang et al., 2023) although smaller ozone changes are due to altered chemical processes (Wilmouth et al., 2023). As noted above, there are two components to the changes in the transport circulation from climatology. The first is natural variability associated with the QBO and year-to-year variability stratospheric wave forcing. The second component is the anomalous circulation produced by the in situ radiative cooling associated with the water vapor anomaly.

As discussed in Section 3.1, ozone changes at the equator (Figures 1c and 3b) are due to the descending westerly and then easterly QBO phases. In the SH extra-tropics, a decrease in ozone occurs from March 2022 through

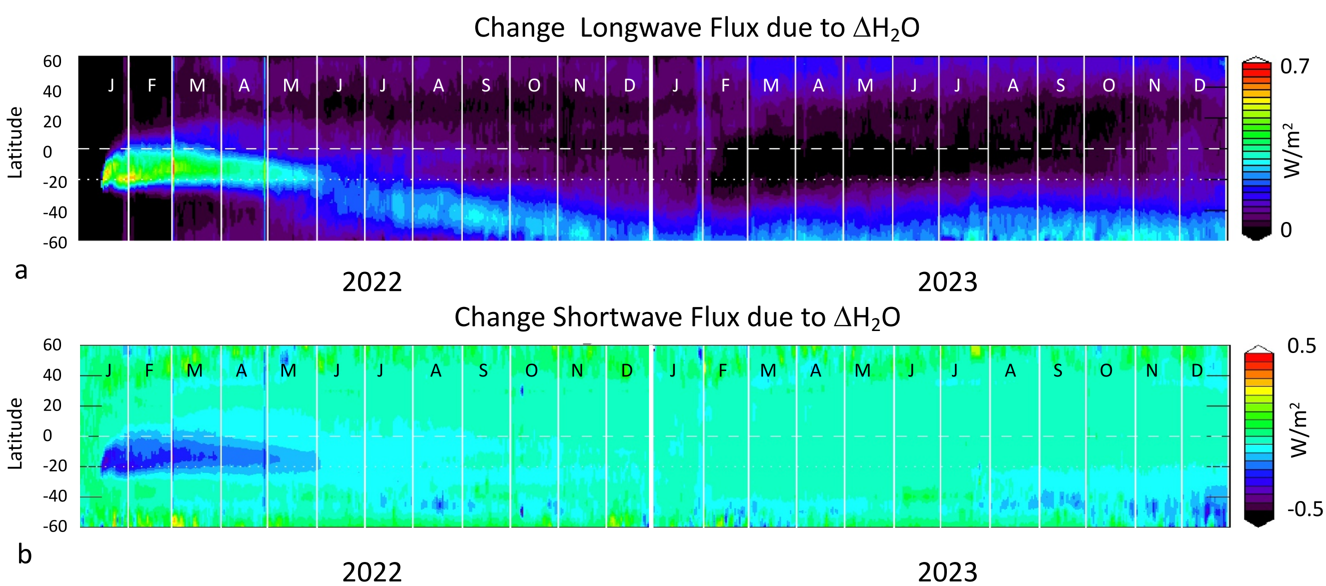

Figure 6. Part a, changes in tropopause long-wave water vapor IR flux from. The tropopause varies from about ~16 km in the tropics (±25°) to ~9 km at extra-tropical latitudes. Part b, change in short-wave flux. Months indicated as in Figure 1.

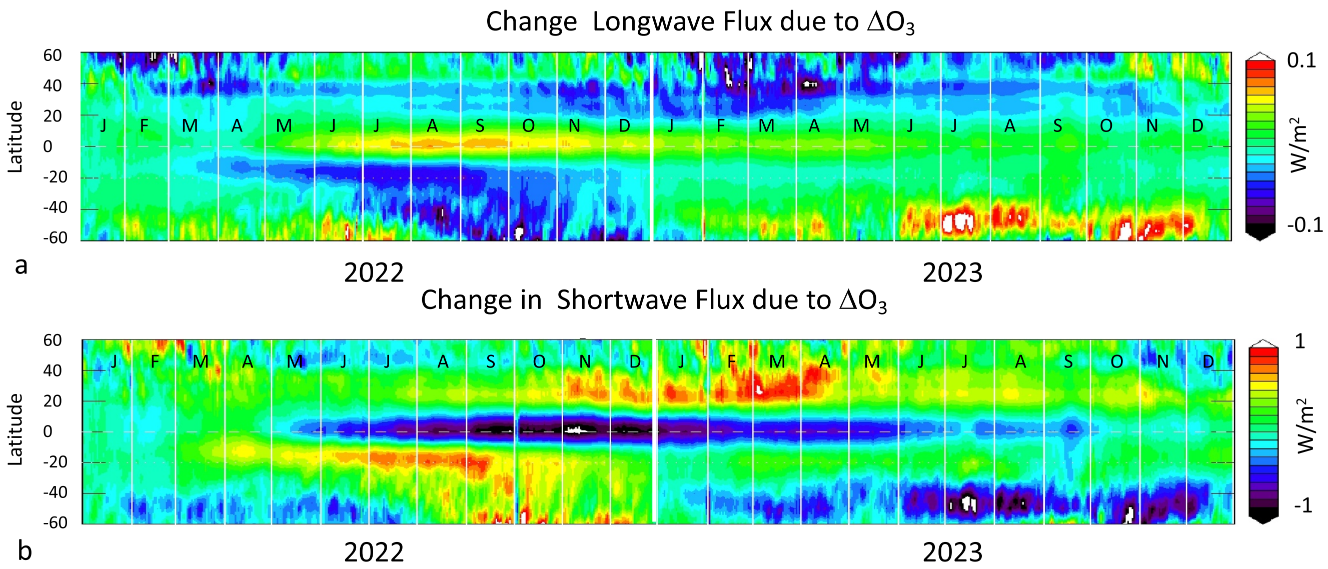

Figure 7. Tropopause fluxes due to change in ozone, Part a, longwave, Part b, shortwave.

October 2022 due to the Hunga induced weakening of the downward branch of the downward BD circulation (Coy et al., 2022; Wang et al., 2023).

Increases in ozone should cause a decrease in shortwave tropopause flux and an increase in longwave tropopause flux and vice versa. As expected, Figure 7a shows a small increase in equatorial downward longwave IR flux associated with the QBO driven ozone enhancement. A larger broader decrease in the SH extra-tropical IR flux is associated with the southern extra-tropical ozone decrease. The longwave ozone flux changes are small relative to the water vapor long wave flux changes (Figure 6b). In contrast, Figure 7b shows the shortwave flux changes are larger than the water vapor shortwave flux changes. The equatorial short-wave ozone flux changes are also mostly associated with the QBO with a relatively large flux decrease at the equator and a smaller flux increase in the southern extratropical latitudes. The shortwave ozone flux changes are on the scale of the aerosol flux changes (Figure 5).

3.3.3. Flux Changes Due To Temperature

The changes in stratospheric temperature also alter the downward longwave fluxes by radiatively important trace gases even though the gas concentrations are not significantly altered by the eruption (e.g., N_2O see Santee et al. (2023), Figure 1). To estimate the tropopause downward flux changes due to temperature changes, we use the climatological trace gas concentration and swap in the 2,022/3 temperatures. Figure 3a shows the 25 km temperature differences from climatology.

Figure 8 shows the temperature induced change in downward longwave fluxes. The shortwave flux is not directly affected by the temperature changes and is not shown. The flux changes roughly mirror the temperature anomalies shown in Figure 3a, especially the impact of the extra-tropical SH cooling from March 2022 - November 2022.

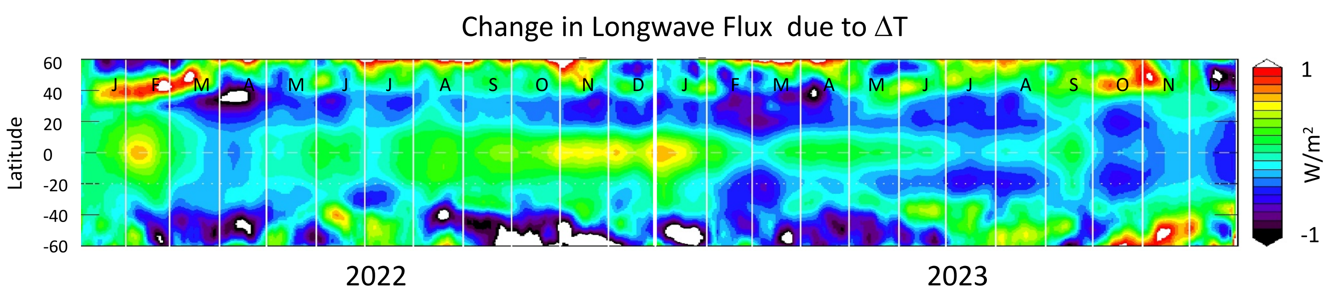

Figure 8. As in Figure 7a but for change in temperature.

Relative to climatology, lower stratospheric temperatures reduce the downward flux and warmer temperatures increase the downward flux. As mentioned in Section 3.1, the SH 2022 temperature anomaly is due to the weaker BD circulation. Changes in downward fluxes due to the stratospheric temperature anomalies are as large or larger than the flux changes due to the trace gas anomalies.

3.4. Combined Fluxes

3.4.1. Total Flux Changes

Figure 9 shows the total estimated tropopause flux changes following the Hunga eruptions. We combine the temperature and trace gas shortwave and longwave downward fluxes with the aerosol direct forcing changes. As with the aerosol direct forcing, short wave forcing by ozone and water vapor is weighted by the solar zenith angle.

Figure 9a shows the zonal mean flux versus time using the NASA OMPS SAOD, while Figure 9b shows the zonal mean fluxes using the USask OMPS SAOD, and parts 9c-e show the component fluxes at the equator, 20°S and 40°S associated with Figure 9a. The component picture shows aerosols dominating the forcing with changes in temperature and ozone (short wave) contributing next. Overall, the long-wave water vapor flux increase, the focus of Jenkins et al. (2023), appears to be one of the least important components of the total flux after the first few months.

Figure 9 shows that there is a net SH radiative flux decrease through most of the 2 yrs period using either NASA or USask SAOD. The exception is near 20° S in Figures 9b–9d where the fluxes are slightly positive August–November 2022. This is the period where the aerosol distribution shifts southward and the increase in ozone short-wave flux exceeds the aerosol flux reduction. Aerosols and short-wave flux variations in ozone and long wave flux variations in temperature dominate the total flux changes.

Figure 4a shows that the Hunga SAOD anomaly persists into the beginning of 2,023 then reaches a small second peak at higher latitudes in May 2023. This second peak shows up in the forcing (Figures 9a–9e). The combination of aerosol direct forcing, temperature changes and ozone recovery lead to net decrease in downward flux in 2023. By the end of 2,023 the aerosol forcing has dwindled to near zero. Fluctuations in the late 2023 forcing components, aside from aerosols, appear to be mostly due to year-to-year variability.

3.4.2. All Sky Albedo

As described above, Yu and Huang (2023) developed a cloud correction for SAOD direct forcing (All sky albedo) which essentially includes cloud reflection of solar radiation before it can reach the surface. Most papers computing aerosol impact of volcanic emissions or fires do not include cloud effects in computing the direct forcing. In our computation, cloud reflectivity is applied to all the short-wave fluxes. The All sky albedo reduces the shortwave ozone and water vapor forcing as well as the aerosol direct effect. Figure 10a shows the impact of All sky albedo on the total forcing using NASA SAOD, and Figure 10b shows the results using USask SAOD. These figures should be compared to Figures 9a and 9b, respectively. The USask SAOD case shows the smallest net forcing, as expected.

3.4.3. Global and Hemispheric Forcing

To estimate the global forcing, we integrate the downward flux from ±60° and remove the forcing estimates from Jan 1-14, 2022, to focus on the relative anomalies. The hemispheric flux is computed from 60° S to the equator and from the equator to 60° N. In Figure 11 we show the two extreme cases—NASA OMPS SAOD clear skies and USask OMPS with all sky albedo to provide an estimate of the uncertainty in the forcing. The two cases are shown in Figures 9a and 10b. The 2,022/2,023 peak and average radiative forcing is summarized in Table 2.

Our results show that during most of the Hunga period there is global net cooling, except for the Jan-Feb. 2022 period right after the eruption, when the water vapor forcing peaked, and before most of the aerosol shroud has formed. A second region of very slightly positive forcing occurs between 10°S and 40°S June-December 2022 where decreases in ozone generate an increase in tropopause shortwave flux.

The Jan-Feb. 2022 global flux increases occurs when a NH warming– not connected with Hunga (Figure 3a) - exceeds the SH cooling. We also note that from Figures 9 and 10 and Table 2, the aerosol reduction in direct forcing is largest in the SH to which the aerosols are confined through most of the post eruption period (Figure 5).

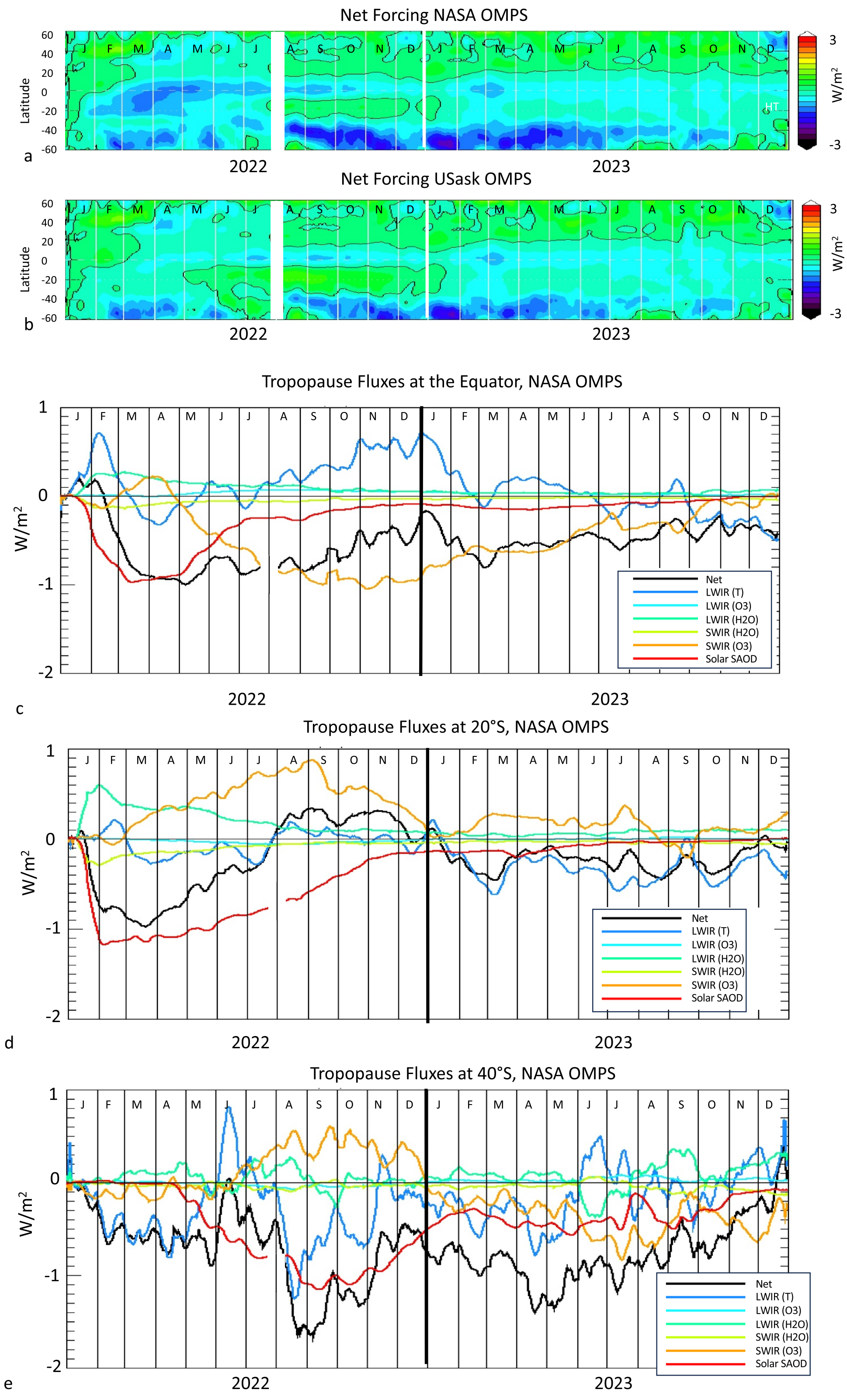

Figure 9. Part (a) Net forcing including trace gas fluxes and aerosol direct forcing using NASA OMPS SAOD at the tropopause. Part b is similar to Part a but for USask SAOD. Parts c, d, e show the various flux components at the equator (Part b), 20°S (Part c) and 40°S (Part d) using NASA OMPS SAOD. The tropopause varies from about ∼16 km in the tropics (±25°) to ∼9 km at extra-tropical latitudes.

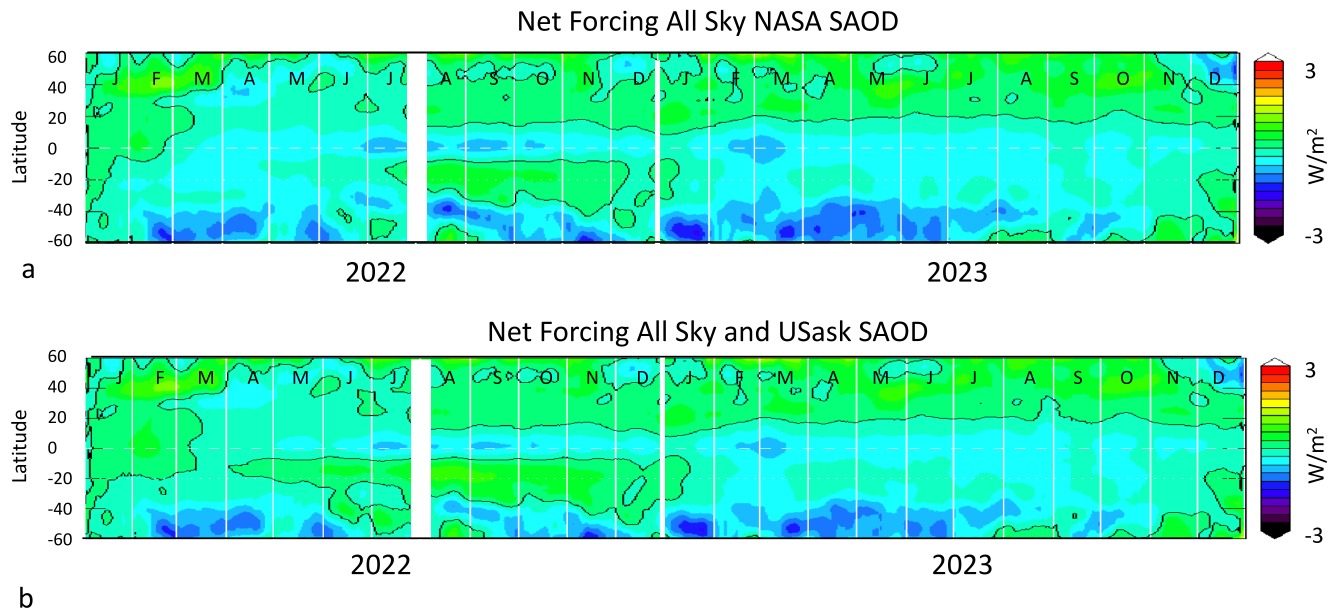

Figure 10. Net forcing using all sky albedo. Part a with NASA OMPS SAOD. Part b, USask OMPS SAOD.

We conclude that the Hunga peak global forcing is -0.475 ± 0.145 W/m^2. In contrast, the Pinatubo global forcing was ~ -3.5 W/m^2 (Pitari et al., 2016), about 6–12 times larger than Hunga.

4. Summary and Conclusions

We have extended the S23b estimate of the Hunga radiative forcing through 2,023. We have also added long-wave and short-wave ozone and long-wave temperature radiative flux changes to our estimates. We note that

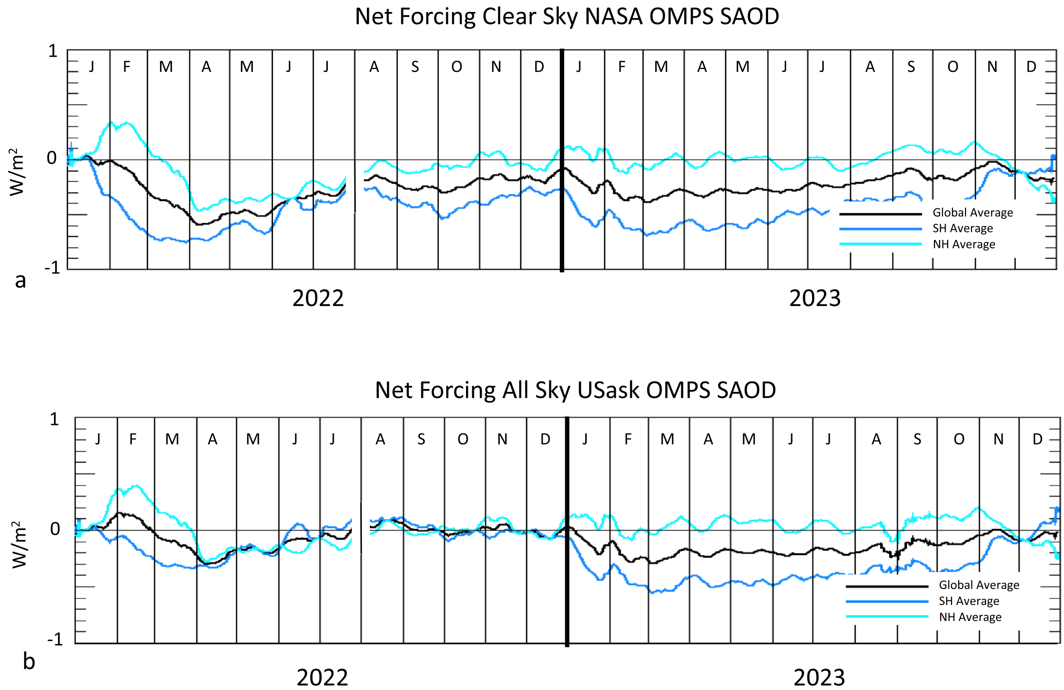

Figure 11. Variations of global (black), SH (blue) and NH (cyan) downward fluxes. Part a, clear sky, NASA OMPS SAOD (see Figure 9a). Part b, all sky USask SAOD (see Figure 10b).

Table 2
Forcing Amounts in W/m^2—Averages Are for 2022-2023

Forcing	Peak global	Peak SH	Peak NH	Average global	Average SH	Average NH
NASA OMPS Clear Sky	−0.59	−0.75	−0.47	−0.24	−0.43	−0.05
USask OMPS All Sky	−0.3	−0.55	−0.39	−0.1	−0.21	0.01
Average	−0.47 ± 0.14	−0.65 ± 0.10	−0.43 ± 0.04	−0.17 ± 0.07	−0.32 ± 0.11	−0.025 ± 0.02

there are post-Hunga differences between the SAOD estimates from NASA OMPS retrievals (Taha et al., 2021) and USask tomographic retrievals (Bourassa et al., 2023). Both retrievals show bias compared to SAGE III/ISS SAOD measurements (Figure 4d) in the first half of 2,022. After mid 2,022 the NASA and USask algorithms are in better agreement. We account for the SAOD differences by performing radiative forcing estimates for both NASA and USask SAOD retrievals as a measure of the forcing uncertainty. We also approximately account for tropospheric cloud albedo using the Yu and Huang (2023) parameterization as was done is S23b.

Our earlier conclusion (S23b) that the 2,022/2,023 global Hunga impact is a reduction in tropopause flux remains valid even with the aerosol uncertainty and ozone/temperature effects included. As we previously found, the tropopause flux reduction is largely due to the aerosol shroud which is mostly confined to the SH. Hunga induced SH lower stratospheric temperature changes (Santee et al., 2023; Wang et al., 2023) reinforce the reduction downward long-wave radiative flux. Stratospheric ozone reduction produces an increase in the shortwave flux, and this is an important contributor to the total flux. In other words, the weakened BD circulation induced by stratospheric water vapor cooling altered the stratospheric temperature and ozone distribution which significantly contributed to Hunga changes in the climate forcing. By the end of 2,023 aerosols have settled out, the water vapor anomaly has largely dispersed in the lower stratosphere, and the Hunga net forcing between ±60° has dissipated.

The Hunga eruption cooled the climate, but the amount of cooling is so small it will be difficult to extract the signal from tropospheric meteorological observations.

Data Availability Statement

The RTM used to estimate H_2O IR cooling rates is from Atmospheric and Environmental Research (RTE + RRTMGP) and can be freely downloaded at http://rtweb.aer.com/rrtm_frame.html.

OMPS data, Taha et al. (2021), is available at https://disc.gsfc.nasa.gov/datasets/OMPS_NPP_LP_L2_AER_DAILY_2/summary, DOI: https://doi.org/10.5067/CX2B9NW6FI27. The algorithm is documented in Taha et al. (2021). Data are public with unrestricted access (registration required).

The OMPS USask data is available at https://doi.org/10.5281/zenodo.7293121.

Aura MLS Level 2 data, Livesey et al. (2021) JPL D-33509 Rev. C, is available at https://disc.gsfc.nasa.gov/datasets?page=1&keywords=AURA%20MLS.

The MLS temperature data is available at https://acdisc.gesdisc.eosdis.nasa.gov/data/Aura_MLS_Level2/ML2T.004/.

The MLS V5 water vapor data is available at https://acdisc.gesdisc.eosdis.nasa.gov/data/Aura_MLS_Level2/ML2H2O.005/.

Acknowledgments
This work was supported under NASA grants NNX14AF15G, 80NSSC21K1965, 80NSSC20K1235, and 80NSSC23K1037. D. Zawada acknowledges the support of the Canadian Space Agency.

References

Aubry, T. J., Staunton-Sykes, J., Marshall, L. R., Haywood, J., Abraham, N. L., & Schmidt, A. (2021). Climate change modulates the stratospheric volcanic sulfate aerosol lifecycle and radiative forcing from tropical eruptions. *Nature Communications*, *12*(1), 4708. https://doi.org/10.1038/s41467-021-24943-7

Banerjee, A., Chiodo, G., Previdi, M., Ponater, M., Conley, A. J., & Polvani, L. M. (2019). Stratospheric water vapor: An important climate feedback. *Climate Dynamics*, *53*(3–4), 1697–1710. https://doi.org/10.1007/s00382-019-04721-4

Bourassa, A. E., Zawada, D. J., Rieger, L. A., Warnock, T. W., Toohey, M., & Degenstein, D. A. (2023). Tomographic retrievals of Hunga Tonga-Hunga Ha'apai volcanic aerosol. *Geophysical Research Letters*, *50*(3), e2022GL101978. https://doi.org/10.1029/2022GL101978

Carn, S. A., Krotkov, N. A., Fisher, B. L., & Li, C. (2022). Out of the blue: Volcanic SO_2 emissions during the 2021-2022 Hunga Tonga – Hunga Ha'apai eruptions, front. Earth sci., 13. *Frontiers in Earth Science*, *10*. https://doi.org/10.3389/feart.2022.976962

Carr, J. L., Horváth, A., Wu, D., & Friberg, M. (2022). Stereo plume height and motion retrievals for the record-setting Hunga Tonga-Hunga Ha'apai eruption of 15 January 2022. *Geophysical Research Letters*, *49*(9), e2022GL098131. https://doi.org/10.1029/2022GL098131

Cisewski, M., Zawodny, J., Gasbarre, J., Eckman, R., Topiwala, N., Rodriguez-Alvarez, O., et al. (2014). The stratospheric aerosol and gas experiment (SAGE III) on the International Space Station (ISS) mission. In. *Sensors, systems, and next-generation satellites xviii*, *9241*, 59–65. SPIE.

Coy, L., Newman, P., Wargan, K., Partyka, G., Strahan, S., & Pawson, S. (2022). Stratospheric circulation changes associated with the Hunga Tonga-Hunga ha'apai eruption. *Geophysical Research Letters*, *49*. https://doi.org/10.1002/essoar.10512388.1

Crutzen, P. J. (2006). Albedo enhancement by stratospheric sulfur injections: A contribution to resolve a policy dilemma? *Climatic Change*, *77*(3–4), 211–220. https://doi.org/10.1007/s10584-006-9101-y

Dessler, A. E., Schoeberl, M. R., Wang, T., Davis, S., & Rosenlof, K. H. (2013). Stratospheric water vapor feedback. *PNAS*, *110*(45), 18087–18091. https://doi.org/10.1073/pnas.1310344110

Forster, P. M. D., & Shine, K. P. (1999). Stratospheric water vapour changes as a possible contributor to observed stratospheric cooling. *Geophysical Research Letters*, *26*(21), 3309–3312. https://doi.org/10.1029/1999gl010487

Fujiwara, M., Martineau, P., & Wright, J. S. (2020). Surface temperature response to the major volcanic eruptions in multiple reanalysis data sets. *Atmospheric Chemistry and Physics*, *20*(1), 345–374. https://doi.org/10.5194/acp-20-345-2020

Gelaro, R., McCarty, W., Suárez, M. J., Todling, R., Molod, A., Takacs, L., et al. (2017). The Modern-Era Retrospective analysis for Research and Applications, version 2 [dataset], (Vol. *30*, pp. 5419–5454). https://doi.org/10.1175/jcli-d-16-0758.1. *Journal of Climate*. (14).

Gorkavyi, N., Krotkov, N., Li, C., Lait, L., Colarco, P., Carn, S., et al. (2021). Tracking aerosols and SO2 clouds from the raikoke eruption: 3D view from satellite observations. *Atmospheric Measurement Techniques*, *14*(12), 7545–7563. https://doi.org/10.5194/amt-14-7545-2021

Hansen, J., Sato, M., Nazarenko, L., Ruedy, R., Lacis, A., Koch, D., et al. (2002). Climate forcings in goddard institute for space studies SI2000 simulations. *Journal of Geophysical Research*, *107*(D18), 4347. https://doi.org/10.1029/2001JD001143

Jenkins, S., Smith, C., Allen, M., & Grainger, R. (2023). Tonga eruption increases chance of temporary surface temperature anomaly above 1.5°C. *Nature Climate Change*, *13*(2), 127–129. https://doi.org/10.1038/s41558-022-01568-2

Khaykin, S. M., de Laat, A. T. J., Godin-Beekmann, S., Hauchecorne, A., & Ratynski, M. (2022). Unexpected self-lofting and dynamical confinement of volcanic plumes: The raikoke 2019 case. *Scientific Reports*, *12*(1), 22409. 2022. https://doi.org/10.1038/s41598-022-27021-0

Li, F., & Newman, P. (2020). Stratospheric water vapor feedback and its climate impacts in the coupled atmosphere–ocean Goddard Earth Observing System Chemistry-Climate Model. *Climate Dynamics*, *55*(5–6), 1585–1595. https://doi.org/10.1007/s00382-020-05348-6

Livesey, N., Read, W. G., Wagner, P. A., Froidevaux, L., Santee, M. L., Schwartz, M. J., et al. (2021). Earth observing System (EOS) aura Microwave limb sounder (MLS) version 5.0x level 2 and 3 data quality and description document, JPL D-105336 Rev A. https://mls.jpl.nasa.gov/data/v5-0_data_quality_document.pdf

Millán, L., Santee, M. L., Lambert, A., Livesey, N. J., Werner, F., Schwartz, M. J., et al. (2022). The Hunga Tonga-Hunga Ha'apai hydration of the stratosphere. *Geophysical Research Letters*, *49*, e2002GL099381. https://doi.org/10.1029/2022GL099381

Millán, L., Read, W. G., Santee, M. L., Lambert, A., Manney, G. L., Neu, J. L., et al. (2024). The evolution of the Hunga hydration in a moistening stratosphere. *Geophysical Research Letters*, *51*, submitted, https://doi.org/10.22541/essoar.171201070.05823623/v1

Mlawer, E. J., Taubman, S. J., Brown, P. D., Iacono, M. J., & Clough, S. A. (1997). RRTM, a validated correlated-k model for the longwave. *Journal of Geophysical Research*, *102*(D14), 16663–16682. https://doi.org/10.1029/97jd00237

Pitari, G., Di Genova, G., Mancini, E., Visioni, D., Gandolfi, I., & Cionni, I. (2016). Stratospheric aerosols from major volcanic eruptions: A composition-climate model study of the aerosol cloud dispersal and e-folding time, atmosphere, 7. *Atmosphere*, *7*(6), 75. https://doi.org/10.3390/atmos7060075

Plumb, R. A., & Bell, R. C. (1982). A model of the quasi-biennial oscillation on an equatorial beta-plane, Quart. *Journal R. Met. Soc.*, *108*(456), 335–352. https://doi.org/10.1256/smsqj.45603

Proud, S., Prata, A., & Schmauß, S. (2022). The January 2022 eruption of Hunga Tonga-Hunga Ha'apai volcano reached the mesosphere. *Science*, *378*(6619), 554–557. https://doi.org/10.1126/science.abo4076

Robock, A. (2000). Volcanic eruptions and climate, revs. Of geophysics. *Reviews of Geophysics*, *38*(2), 191–219. https://doi.org/10.1029/1998RG000054

Santee, M. L., Lambert, A., Froidevaux, L., Manney, G. L., Schwartz, M. J., Millán, L. F., et al. (2023). Strong evidence of heterogeneous processing on stratospheric sulfate aerosol in the extra-polar Southern Hemisphere following the 2022 Hunga Tonga-Hunga Ha'apai eruption. *Journal of Geophysical Research: Atmospheres*, *128*(16), e2023JD039169. https://doi.org/10.1029/2023JD039169

Santer, B. D., Wigley, T. M. L., Doutriaux, C., Boyle, J. S., Hansen, J. E., Jones, P. D., et al. (2001). Accounting for the effects of volcanoes and ENSO in comparisons of modeled and observed temperature trends. *Journal of Geophysical Research*, *106*(D22), 28033–28059. https://doi.org/10.1029/2000JD000189

Schoeberl, M. R., Wang, Y., Ueyama, R., Dessler, A., Taha, G., & Yu, W. (2023). The estimated climate impact of the Hunga Tonga-Hunga Ha'apai eruption plume. *Geophysical Research Letters*, *50*(18), e2023GL104634. https://doi.org/10.1029/2023GL104634

Schoeberl, M. R., Wang, Y., Ueyama, R., Taha, G., Jensen, E., & Yu, W. (2022). Analysis and impact of the Hunga Tonga-Hunga Ha'apai stratospheric water vapor plume. *Geophysical Research Letters*, *49*(20), e2022GL100248. https://doi.org/10.1029/2022GL100248

Schoeberl, M. R., Wang, Y., Ueyama, R., Taha, G., & Yu, W. (2023). The cross equatorial transport of the Hunga Tonga-Hunga ha'apai eruption plume. *Geophysical Research Letters*, *49*(4), e2022GL10443. https://doi.org/10.1029/2022GL102443

Sellitto, P., Podglagen, A., Belhadji, R., Boichu, M., Carboni, E., Cuesta, J., et al. (2022). The unexpected radiative impact of the Hunga Tonga eruption of January 15, 2022, Commun. *Earth and Environment*, *3*(2022), 288. https://doi.org/10.1038/s43247-022-00618-z

Sellitto, P., Siddans, R., Belhadji, R., Carboni, E., Legras, B., Podglajen, A., et al. (2024). Observing the SO2 and sulphate aerosol plumes from the 2022 Hunga Tonga-Hunga ha'apai eruption with IASI. submitted to. *Geophysical Research Letters*. https://doi.org/10.22541/essoar.169091894.48592907/v1

Solomon, S., Rosenlof, R., Portmann, J. S., Daniel, S. M. D., Sanford, T. J., Plattner, G.-K., & Plattner, G. K. (2010). Contributions of stratospheric water vapor to decadal changes in the rate of global warming. *Science*, *237*(5970), 1219–1221. https://doi.org/10.1126/science.1182488

Stenchikov, G. (2016). *The role of volcanic activity in climate and global change* (2nd ed.). Elsevier. https://doi.org/10.1016/B978-0-444-63524-2.00026-9

Taha, G., Loughman, R., Colarco, P., Zhu, T., Thomason, L., & Jaross, G. (2022). Tracking the 2022 Hunga Tonga-Hunga Ha'apai aerosol cloud in the upper and middle stratosphere using space-based observations, Geophy. Res. Lett. *Geophysical Research Letters*, *49*(19). https://doi.org/10.1029/2022GL100091

Taha, G., Loughman, R., Zhu, T., Thomason, L., Kar, J., Rieger, L., & Bourassa, A. (2021). OMPS LP Version 2.0 multi-wavelength aerosol extinction coefficient retrieval algorithm. *Atmospheric Measurement Techniques*, *14*(2), 1015–1036. https://doi.org/10.5194/amt-14-1015-2021

Tao, M., Konopka, P., Ploeger, F., Grooß, J. U., Müller, R., Volk, C. M., et al. (2015). Impact of the 2009 major sudden stratospheric warming on the composition of the stratosphere. *Atmospheric Chemistry and Physics*, *15*(15), 8695–8715. https://doi.org/10.5194/acp-15-8695-2015

Veenus, V., Das, S. S., & David, L. M. (2023). Ozone changes due to sudden stratospheric warming-induced variations in the intensity of brewer-dobson circulation: A composite analysis using observations and chemical-transport model. *Geophysical Research Letters*, *50*(13), e2023GL103353. https://doi.org/10.1029/2023GL103353

Vömel, H., Evan, S., & Tully, M. (2022). Water vapor injection into the stratosphere by Hunga Tonga-Hunga Ha'apai. *Science*, *377*(6613), 1444–1447. https://doi.org/10.1126/science.abq2299

Wang, X., Randel, W., Zhu, Y., Tilmes, S., Starr, J., Yu, W., et al. (2023). Stratospheric climate anomalies and ozone loss caused by the Hunga Tonga-Hunga Ha'apai volcanic eruption. *Journal of Geophysical Research: Atmospheres*, *128*(22), e2023JD039480. https://doi.org/10.1029/2023JD039480

Wilmouth, D., Østerstrøm, F., Smith, J., Anderson, J. G., & Salawitch, R. (2023). Impact of the Hunga Tonga volcanic eruption on stratospheric composition. *PNAS*, *120*(46), e2301994120. https://doi.org/10.1073/pnas.2301994120

Yu, Q., & Huang, Y. (2023). Distributions and trends of the aerosol direct radiative effect in the 21st century: Aerosol and environmental contributions. *Journal of Geophysical Research: Atmospheres*, *128*(4), e2022JD037716. https://doi.org/10.1029/2022JD037716

Yu, W., Garcia, R., Yue, J., Smith, A., Wang, X., Randel, W., et al. (2023). Mesospheric temperature and circulation response to the Hunga Tonga-Hunga Ha'apai volcanic eruption. *Journal of Geophysical Research: Atmospheres*, *128*(21), e2023JD039636. https://doi.org/10.1029/2023JD039636

Zhu, Y., Bardeen, C. G., Tilmes, S., Mills, M. J., Wang, X., Lynn Harvey, V., et al. (2022). Perturbations in stratospheric aerosol evolution due to the water-rich plume of the 2022 Hunga-Tonga eruption. *Communications Earth & Environment*, *3*(1), 248. https://doi.org/10.1038/s43247-022-00580-w